MOX-Report No. 18/2021

On the choice of interface parameters in Robin-Robin loosely coupled schemes for fluid-structure interaction

Gigante, G.; Vergara, C.

MOX, Dipartimento di Matematica
Politecnico di Milano, Via Bonardi 9 - 20133 Milano (Italy)

mox-dmat@polimi.it http://mox.polimi.it

On the choice of interface parameters in Robin-Robin loosely coupled schemes for fluid-structure interaction

G. Gigante[1], C. Vergara[2]

March 16, 2021

[1] Dipartimento di Ingegneria Gestionale, dell'Informazione e della Produzione
Università degli Studi di Bergamo, Italy
giacomo.gigante@unibg.it

[2] LABS, Dipartimento di Chimica, Materiali e Ingegneria Chimica "Giulio Natta"
and Adjunct Professor at MOX, Dipartimento di Matematica
Politecnico di Milano, Italy
christian.vergara@polimi.it

Keywords: Fluid-structure interaction; loosely-coupled scheme; Robin interface condition; Optimized Schwarz Method

AMS Subject Classification: 65N12, 65N30

Abstract

We consider two loosely-coupled schemes for the solution of the fluid-structure interaction problem in presence of large added mass effect. In particular, we introduce the Robin-Robin and Robin-Neumann explicit schemes where suitable interface conditions of Robin type are used. For the estimate of interface Robin parameters which guarantee stability of the numerical solution, we propose to optimize the reduction factor of the corresponding strongly-coupled (implicit) scheme, by means of the Optimized Schwarz method. To check the suitabilty of our proposals, we show numerical results both in an ideal cylindrical domain and in a real human carotid.

1 Introduction

Loosely-coupled schemes for the numerical solution of the fluid-structure interaction (FSI) problem are based on an overall explicit time discretization which leads to the solution of just one fluid and one structure problem per time step. This makes this family of methods very attractive from the computational and implementative point of view and for these reasons have been widely

used in many engineering applications such as aeroelasticity [11, 29, 30]. However, loosely-coupled schemes suffer from a lack of stability when the *added mass effect* is relevant (i.e. when the densities of fluid and structure are comparable). This happens for example in hemodynamics [31]. In this respect, it is known that the explicit *Dirichlet-Neumann* (DN) scheme is unconditionally unstable in the hemodynamic regime, see [8, 15, 28].

Recently, some studies introduced loosely-coupled schemes for the FSI problem based on Robin interface conditions, obtained by considering linear combinations of the no-slip condition and action-reaction principle by means of suitable parameters [4–7, 12, 13, 21, 23, 27]. In such works different proposal for the interface parameters were addressed with the aim of improving the stability properties when the added mass effect is relevant with respect to the explicit DN scheme. In our recent study [20], we have provided for a model problem a stability analysis of the explicit *Robin-Neumann* (RN) scheme. In particular, we have found sufficient conditions for the interface Robin parameter guaranteeing both unconditional instability and conditional stability.

In this paper, we address the issue of selecting suitable and easily computable interface parameters both for the explicit RN and the explicit *Robin-Robin* (RR) schemes, able to guarantee the stability of such loosely-coupled schemes. In particular, we discuss the case of clyndrical-like geometries as happens for example in vascular hemodynamics. We start from the analysis based on the *Optimized Schwarz Method* [16] provided for the implicit (i.e. strongly coupled) RR scheme in the FSI context in [19]. This allowed us to determine effective values for the Robin interface parameters which guarantee excellent converge property even in presence of large added mass effect[1]. Here we provide also a new way to easily estimate an effective Robin interface parameter for the RN strongly-coupled scheme. The idea of the present work is to use such estimates in the corresponding loosely-coupled RN and RR schemes. In particular, we verify the stability of the corresponding numerical solution in 3D FSI numerical experiments.

2 Mathematical and numerical setting

2.1 The continuous problem

We consider the coupling between the Navier-Stokes equations for an incompressible fluid solved in the *Arbitrary Lagrangian-Eulerian* (ALE) formulation [10] and the linear infinitesimal elasticity. Let Ω_f and Ω_s be the fluid and structure domains, Σ the fluid-structure interface, Σ^{out} the external structure surface, $\boldsymbol{n} = \boldsymbol{n}_f$ the unit normal outgoing the fluid domain, and $\boldsymbol{n}_s$ the unit normal

[1] For strongly-coupled scheme, a large added mass effect yields a very slow convergence [8]

outgoing the structure domain. We have for each t:

$$\begin{aligned}
&\rho_f \partial_t^A \boldsymbol{u} + \rho_f((\boldsymbol{u}-\boldsymbol{\omega})\cdot\nabla)\boldsymbol{u} - \nabla\cdot\boldsymbol{T}_f(\boldsymbol{u},p) = \boldsymbol{0} && \text{in } \Omega_f,\\
&\nabla\cdot\boldsymbol{u} = 0 && \text{in } \Omega_f,\\
&\boldsymbol{u} = \delta_t\boldsymbol{\eta} && \text{on } \Sigma,\\
&\boldsymbol{T}_f\boldsymbol{n} - \boldsymbol{T}_s\boldsymbol{n} = \boldsymbol{0} && \text{on } \Sigma,\\
&\rho_s \partial_{tt}\widehat{\boldsymbol{\eta}} - \nabla\cdot\widehat{\boldsymbol{T}}_s(\widehat{\boldsymbol{\eta}}) = \boldsymbol{0} && \text{in } \widehat{\Omega}_s, \qquad (1a)\\
&\gamma_{ST}\widehat{\boldsymbol{\eta}} + \widehat{\boldsymbol{T}}_s(\widehat{\boldsymbol{\eta}})\boldsymbol{n}_s = 0 && \text{on } \widehat{\Sigma}^{out}, \qquad (1b)
\end{aligned}$$

where $\boldsymbol{T}_f(\boldsymbol{u},p) = -p\boldsymbol{I} + \mu(\nabla\boldsymbol{u} + (\nabla\boldsymbol{u})^T)$ is the Cauchy stress tensor for the fluid and with μ the dynamic viscosity. ∂_t^A represents the ALE time derivative, i.e. with respect to the ALE framework, and $\boldsymbol{\omega}$ is the velocity of the fluid domain obtained by solving an harmonic extension of the interface velocity with homogeneous Dirichlet or Neumann boundary conditions on $\Omega_f \setminus \Sigma$. Notice that, accordingly, Ω_f changes in time. Instead, the structure problem (1a) is solved in a Lagrangian framework and for this reason we have indicated with $\widehat{\ }$ the corresponding quantities. For the sake of notation, in what follows $\widehat{\ }$ will be understood. Moreover, $\boldsymbol{T}_s$ is the structure Cauchy stress tensor given by

$$\boldsymbol{T}_s(\boldsymbol{\eta}) = \lambda_1(\nabla\boldsymbol{\eta} + (\nabla\boldsymbol{\eta})^T) + \lambda_2(\nabla\cdot\boldsymbol{\eta})\boldsymbol{I},$$

where λ_1 and λ_2 are the Lamé constants, that can be defined in terms of the Young modulus E and the Poisson ratio ν as follows

$$\lambda_1 = \frac{E}{2(1+\nu)}, \quad \lambda_2 = \frac{\nu E}{(1+\nu)(1-2\nu)}.$$

Finally, we observe that condition (1b) represents a Robin condition at the external surface to account for the effect of an elastic surrounding tissue with elasticity modulus γ_{ST} [24]. The previous problem needs to be completed with other boundary conditions and initial conditions for both fluid and structure.

2.2 Robin-Robin loosely-coupled scheme

In order to write a suitable algorithm for the numerical solution of the FSI problem (1), we first need to detail the time discretizaton and how we manage the geometric coupling, i.e. the fact that the fluid domain movement depends on the structure displacement. Regarding the time discretization, we used a first order implicit method for both fluid and structure, with a semi-implicit treatment of the fluid convective term, relying on a CFL-like bound for the time discretization Δt. We also consider an explicit treatment of the no-slip condition, allowing in fact to split the two subproblems. Regarding the geometric coupling, it has been shown that in the hemodynamic regime an explicit treatment is enough to provide stable and accurate results [3, 14, 26, 27, 32]. This means that the harmonic extension problem for the fluid domain displacement and velocity

is solved with structure data that comes from previous time steps. This in fact decouples the geometric and FSI problems, thus at each time step the time discretization of problem (1) is in fact solved in a known domain Ω_f.

Let $t^n = n\Delta t$, $n = 0, \ldots,$ the discrete time instants and $v^n \simeq v(t^n)$ the approximation at time t^n of a function of time $v(t)$. Thus, for the numerical solution of this problem, we introduce the following loosely-coupled scheme:

Algorithm 1 Explicit Robin-Robin scheme

Given two scalars $\alpha_f \neq \alpha_s$ and quantities at previous time steps, at time step t^{n+1} solve in sequence:

1: A fluid problem with a Robin condition at the fluid-structure interface:

$$\rho_f \frac{\boldsymbol{u}^{n+1} - \boldsymbol{u}^n}{\Delta t} + \rho_f((\boldsymbol{u^n} - \boldsymbol{\omega^n}) \cdot \nabla)\boldsymbol{u}^{n+1} - \nabla \cdot \boldsymbol{T}_f(\boldsymbol{u}^{n+1}, p^{n+1}) = \boldsymbol{0} \quad \text{in } \Omega_f^n,$$

$$\nabla \cdot \boldsymbol{u}^{n+1} = 0 \quad \text{in } \Omega_f^n,$$

$$\alpha_f \boldsymbol{u}^{n+1} + \boldsymbol{T}_f(\boldsymbol{u}^{n+1}, p^{n+1})\boldsymbol{n} = \alpha_f \frac{\boldsymbol{\eta}^n - \boldsymbol{\eta}^{n-1}}{\Delta t} + \boldsymbol{T}_s(\boldsymbol{\eta}^n) \quad \text{on } \Sigma^n; \tag{2a}$$

2: A structure problem with a Robin condition at the fluid-structure interface:

$$\rho_s \frac{\boldsymbol{\eta}^{n+1} - 2\boldsymbol{\eta}^n + \boldsymbol{\eta}^{n-1}}{\Delta t^2} - \nabla \cdot \boldsymbol{T}_s(\boldsymbol{\eta}^{n+1}) = \boldsymbol{0} \quad \text{in } \Omega_s^0,$$

$$\alpha_s \boldsymbol{\eta}^{n+1} + \Delta t \boldsymbol{T}_s(\boldsymbol{\eta}^{n+1}) = \alpha_s \Delta t \boldsymbol{u}^{n+1} + \Delta t \boldsymbol{T}_f(\boldsymbol{u}^{n+1}, p^{n+1})\boldsymbol{n} + \alpha_s \boldsymbol{\eta}^n \quad \text{on } \Sigma^0,$$

$$\gamma_{ST} \boldsymbol{\eta}^{n+1} + \boldsymbol{T}_s(\boldsymbol{\eta}^{n+1})\boldsymbol{n}_s = 0 \quad \text{on } \Sigma^{out}.$$

Remark 1. *The implicit (strongly-coupled) Robin-Robin scheme is obtained from Algorithm 1 by replacing the right hand side of* (2a) *with* $\alpha_f \frac{\boldsymbol{\eta}^{n+1} - \boldsymbol{\eta}^n}{\Delta t} + \boldsymbol{T}_s(\boldsymbol{\eta}^{n+1})$ *and then subiterating with the structure problem* (3).

In what follows we discuss the choice of the interface parameters α_f and α_s in the case of cylindrical-like geometries and interface, a situation which occurs in many application with large added mass effect, e.g. in hemodynamics.

3 On the choice of the interface parameters

3.1 Convergence analysis of the implicit Robin-Robin scheme

Our starting point is the optimization procedure to properly select the interface parameters in the implicit Robin-Robin scheme for a simplified FSI problem in the case of cylindrical geometries in [19], whose main results are here reviewed for the sake of completeness.

We consider the problem arising from the interaction between an incompressible, inviscid and linear fluid occupying the fixed domain
$\Omega_f = \{(x_1, x_2, y) \in \mathbb{R}^3 : x_1^2 + x_2^2 < R^2\}$, and a linear elastic structure modeled with the wave equation occupying the domain
$\Omega_s = \{(x_1, x_2, y) \in \mathbb{R}^3 : R^2 < x_1^2 + x_2^2 < (R+H)^2\}$, where
$\Sigma_{out} = \{(x_1, x_2, y) \in \mathbb{R}^3 : x_1^2 + x_2^2 = (R+H)^2\}$ is the external surface. The two subproblems interact at the interface $\Sigma = \{(x_1, x_2, y) \in \mathbb{R}^3 : x_1^2 + x_2^2 = R^2\}$. In Algorithm 2 we report the implicit Robin-Robin scheme at time t^{n+1} for the solution of this simplified FSI problem. Actual temporal index $n+1$ is understood. Notice that the coupling occurs only in the radial direction r since the fluid is inviscid. We have indicated with u_r and η_r the radial fluid velocity and structure displacement, respectively, and with F_1 and F_2 terms coming from the previous time step.

Notice that in [19] we considered general operators $\mathcal{S}_f$ and $\mathcal{S}_s$ to build the interface linear combinations. Here for the sake of exposition, we limit ourselves to the scalar constant case since the forthcoming optimization is performed over the subset of the scalars.

Algorithm 2 Implicit Robin-Robin scheme for the simplified FSI problem

Given two scalars $\alpha_f \neq \alpha_s$ and quantities at previous time steps, solve for $k \geq 1$ until convergence:

1: A fluid problem with a Robin condition at the fluid-structure interface:

$$\rho_f \frac{\boldsymbol{u}^{(k)} - \boldsymbol{u}^n}{\Delta t} + \nabla p^{(k)} = \mathbf{0} \qquad \text{in } \Omega_f,$$
$$\nabla \cdot \boldsymbol{u}^{(k)} = 0 \qquad \text{in } \Omega_f,$$
$$\alpha_f u_r^{(k)} - p^{(k)} = \alpha_f \frac{\eta_r^{(k-1)}}{\Delta t} + \lambda \frac{\partial \eta_r^{(k-1)}}{\partial \boldsymbol{n}} + F_1(u_r^n, \eta_r^n) \qquad \text{on } \Sigma;$$

2: A structure (wave) problem with a Robin condition at the fluid-structure interface:

$$\rho_s \frac{\boldsymbol{\eta}^{(k)} - 2\boldsymbol{\eta}^n + \boldsymbol{\eta}^{n-1}}{\Delta t^2} - \lambda \triangle \boldsymbol{\eta}^{(k)} = \mathbf{0} \qquad \text{in } \Omega_s,$$
$$\alpha_s \eta_r^{(k)} + \Delta t \lambda \frac{\partial \eta_r^{(k)}}{\partial \boldsymbol{n}} = \alpha_s \Delta t u_r^{(k)} - \Delta t p^{(k)} + F_2(u_r^n, \eta_r^n) \qquad \text{on } \Sigma,$$
$$\boldsymbol{\eta}^{(k)} \times \boldsymbol{n} = \mathbf{0} \qquad \text{on } \Sigma,$$
$$\boldsymbol{\eta}^{(k)} \times \boldsymbol{n} = \mathbf{0} \qquad \text{on } \Sigma,$$
$$\gamma_{ST} \boldsymbol{\eta}^{(k)} + \lambda \frac{\partial \boldsymbol{\eta}^{(k)}}{\partial \boldsymbol{n}} = \mathbf{0} \qquad \text{on } \Sigma^{out}.$$

3.2 Selection of effective interface parameters values for the explicit Robin-Robin scheme

Following [19], set

$$A(m,k) = -\frac{\lambda\Delta t\beta\left(K_m'(\beta R) - \chi\, I_m'(\beta R)\right)}{K_m(\beta R) - \chi\, I_m(\beta R)}, \tag{6a}$$

$$B(m,k) = -\frac{\rho_f\, I_m(kR)}{\Delta t\, k\, I_m'(kR)},$$

$$\beta(k) = \sqrt{k^2 + \frac{\rho_s}{\lambda\Delta t^2}}, \tag{6b}$$

$$\chi(m,k) = \frac{\gamma_{ST} K_m\left(\beta(R+H)\right) + \lambda\beta K_m'(\beta(R+H))}{\gamma_{ST} I_m(\beta(R+H)) + \lambda\beta I_m'(\beta(R+H))}, \tag{6c}$$

$$\overline{B} := \max_{(m,k)\in K} B\left(m,k\right), \qquad \overline{A} := \min_{(m,k)\in K} A\left(m,k\right),$$

$$\overline{M} = \frac{1}{2}\left(\overline{A} + \overline{B}\right),$$

$$D\left(m,k\right) = \frac{1}{2}\left(A\left(m,k\right) - B\left(m,k\right)\right), \qquad M\left(m,k\right) = \frac{1}{2}\left(A\left(m,k\right) + B\left(m,k\right)\right),$$

$$Q\left(m,k\right) = \frac{\left|M\left(m,k\right) - \overline{M}\right|}{D\left(m,k\right)},\ \overline{Q} = \sup_{(m,k)\in K} Q\left(m,k\right),\ N = \frac{\inf_{(m,k)\in K} D\left(m,k\right)}{\sup_{(m,k)\in K} D\left(m,k\right)},$$

$$\rho_0 = \max\left\{\left(\frac{1-\sqrt{N}}{1+\sqrt{N}}\right)^2; \left(\frac{1-\sqrt{1-\overline{Q}^2}}{\overline{Q}}\right)^2\right\},$$

where $k \geq 0$ and $m = 0, 1, 2, \ldots$ are the frequencies related to the axial and circumferential coordinates, respectively, and which belong to the set K, I_m and K_m are the modified Bessel functions [22]. Then, in [19] it has been proven, through the Optimized Schwarz Method, that the reduction factor related to Algorithm 2 is given by

$$\rho(m,k) = \left|\frac{\alpha_f - A\left(m,k\right)}{\alpha_s - A\left(m,k\right)} \cdot \frac{\alpha_s - B\left(m,k\right)}{\alpha_f - B\left(m,k\right)}\right|. \tag{7}$$

In particular, it has been proposed to look for parameter values along the straight line $\alpha_f = p$ and $\alpha_s = -p + 2\overline{M}$ for varying $p \in \mathbb{R}$. With this specific choice, the reduction factor (7) becomes

$$\rho(m,k) = \left|\frac{p - A\left(m,k\right)}{2\overline{M} - p - A\left(m,k\right)} \frac{2\overline{M} - p - B\left(m,k\right)}{p - B\left(m,k\right)}\right|,$$

and it has been proved that it satisfies

$$\rho(m,k) \leq \rho_0$$

for any $(m,k) \in K$ if and only if $p \in [p_-, p_+]$ with

$$\begin{aligned} p_- &= \overline{M} \\ &+ \sup_{(m,k)\in K} \left\{ \tfrac{1+\rho_0}{1-\rho_0} D(m,k) - \sqrt{\left(\overline{M} - M(m,k)\right)^2 + \tfrac{4\rho_0}{(1-\rho_0)^2} \left(D(m,k)\right)^2} \right\}, \\ p_+ &= \overline{M} \\ &+ \inf_{(m,k)\in K} \left\{ \tfrac{1+\rho_0}{1-\rho_0} D(m,k) + \sqrt{\left(\overline{M} - M(m,k)\right)^2 + \tfrac{4\rho_0}{(1-\rho_0)^2} \left(D(m,k)\right)^2} \right\}. \end{aligned} \tag{8}$$

The previous result provided an easy way to compute a range of values of p (and thus of α_f and α_s) which guarantees convergence for any frequencies $(m,k) \in K$. Moreover, this range contains the optimal value p^* of p which minimizes the reduction factor for the choice $\alpha_f = p$ and $\alpha_s = -p + 2\overline{M}$, which could be easily found manually. The efficiency of such procedure has been shown in [19] both in ideal and in realistic carotid geometries in the context of hemodynamics. An extension to the case of spherical geometries and interfaces has been provided in [18].

The idea proposed in this paper is to use the range $p \in [p_-, p_+]$ given by (8) to properly select the interface parameters in the explicit Robin-Robin Algorithm 1, still with the specific choice $\alpha_f = p$ and $\alpha_s = -p + 2\overline{M}$. In particular, we propose here to use the optimal value p^* also for the explicit RR scheme. Indeed, we expect that the interface Robin parameters that guarantee a fast convergence in the implicit case should guarantee stability and accuracy for the explicit case. Although there is not yet a proof of this, we provide here an experimental analysis to support our choices, see Section 4.

3.3 An alternative way to select the interface parameter in the explicit Robin-Neumann scheme

We consider now the implicit Robin-Neumann scheme, i.e. Algorithm 2 with $\alpha_s = 0$. We propose here a new way to efficiently select the parameter α_f for this algorithm. In particular, we still look for $\alpha_f = p$ with p a scalar independent of the frequencies.

We have the following result.

Theorem 1. *Suppose to have for a given iterative algorithm a reduction factor of the form*

$$\rho(k) = \left| \frac{p - A(k)}{p - B(k)} \cdot \frac{B(k)}{A(k)} \right|, \tag{9}$$

for suitable scalar functions $A(k)$ and $B(k)$ defined on K, where k is a general

scalar or vector variable, and with $A(k)B(k) \neq 0$ for all $k \in K$. Then, by setting

$$\begin{aligned} a &= \frac{1}{A}, \qquad b = \frac{1}{B}, \\ \overline{a} &= \max_{k\in K} a\left(k\right), \qquad \underline{a} = \min_{k\in K} a\left(k\right), \\ \overline{b} &= \max_{k\in K} b\left(k\right), \qquad \underline{b} = \min_{k\in K} b\left(k\right), \end{aligned}$$

if $\overline{b} < \underline{a}$, we have

$$\rho(k) \leq \theta = \frac{\overline{a} - \underline{a}}{\overline{a} + \underline{a} - 2\overline{b}} < 1, \tag{10}$$

for any $k \in K$ provided that

$$\frac{1}{p} \in \left[\frac{\max_{k\in K}\left(a\left(k\right) + \theta b\left(k\right)\right)}{1+\theta}, \frac{\min_{k\in K}\left(a\left(k\right) - \theta b\left(k\right)\right)}{1-\theta}.\right]. \tag{11}$$

Proof. Notice that for any $\theta \in [0, 1)$ we have

$$\frac{\max_{k\in K}\left(a\left(k\right) + \theta b\left(k\right)\right)}{1+\theta} \leq \frac{\overline{a} + \theta\overline{b}}{1+\theta}$$

and

$$\frac{\underline{a} - \theta\overline{b}}{1-\theta} \leq \frac{\min_{k\in K}\left(a\left(k\right) - \theta b\left(k\right)\right)}{1-\theta}.$$

By imposing

$$\frac{\overline{a} + \theta\overline{b}}{1+\theta} = \frac{\underline{a} - \theta\overline{b}}{1-\theta},$$

i.e. for

$$\theta = \frac{\overline{a} - \underline{a}}{\overline{a} + \underline{a} - 2\overline{b}} \in [0, 1),$$

we can write

$$\frac{\max_{k\in K}\left(a\left(k\right) + \theta b\left(k\right)\right)}{1+\theta} \leq \frac{\min_{k\in K}\left(a\left(k\right) - \theta b\left(k\right)\right)}{1-\theta}. \tag{12}$$

Now, setting

$$q = \frac{1}{p},$$

we can write the reduction factor (9) as follows

$$\rho(k) = \left|\frac{\frac{1}{q} - \frac{1}{a(k)}}{\frac{1}{q} - \frac{1}{b(k)}} \cdot \frac{\frac{1}{b(k)}}{\frac{1}{a(k)}}\right| = \left|\frac{a\left(k\right) - q}{b\left(k\right) - q}\right|.$$

One only has to observe now that inequality (10), that is

$$-\theta \leq \frac{a\left(k\right) - q}{b\left(k\right) - q} \leq \theta$$

is equivalent to

$$\frac{a\,(k)+\theta b\,(k)}{1+\theta} \leq q \leq \frac{a\,(k)-\theta b\,(k)}{1-\theta},$$

which makes sense for any $k \in K$ owing to (12). Thus the thesis follows. □

We can now apply the above result to our case, i.e. the implicit Robin-Neumann scheme (Algorithm 2 with $\alpha_s = 0$), interpreting k in Theorem 1 as the couple of frequencies (m, k) and by taking A and B as in (6a)-(6c). Indeed, from (7), by setting $\alpha_f = p$ and $\alpha_s = 0$, we obtain

$$\rho(m,k) = \left|\frac{p - A\,(m,k)}{-A\,(m,k)} \cdot \frac{-B\,(m,k)}{p - B\,(m,k)}\right| = \left|\frac{p - A\,(m,k)}{p - B\,(m,k)} \cdot \frac{B\,(m,k)}{A\,(m,k)}\right|.$$

We now only need to prove that, as requested by Theorem 1, $\bar{b} < \underline{a}$. To this aim, we prove the following result.

Lemma 1. *For all integers $m \geq 0$ and for all $k \geq 0$, one has*

$$a(m,k) = \frac{1}{A(m,k)} = \frac{K_m(\beta R) - \chi I_m(\beta R)}{\lambda \Delta t \beta(-K'_m(\beta R) + \chi I'_m(\beta R))} > 0$$

and

$$b(m,k) = \frac{1}{B(m,k)} = -\frac{\Delta t k I'_m(|k|R)}{\rho_f I_m(kR)} \leq 0,$$

with β and χ given by (6b) *and*(6c). *When $k = 0$, the expression for $b(m,k)$ has to be intended as $k \to 0$, that is*

$$b(m,0) = -\frac{\Delta t m}{\rho_f R}.$$

Proof. The estimate for $b(m,k)$ is trivial, since both I_m and I'_m are positive functions.

Concerning $a(m,k)$, for notational convenience, set $x = \beta R$, $h = \beta H$, and $c = \lambda\beta/\gamma_{ST}$. The numerator of $a(m,k)$ is positive if and only if

$$\frac{K_m(x)}{I_m(x)} > \chi = \frac{K_m(x+h) + cK'_m(x+h)}{I_m(x+h) + cI'_m(x+h)}.$$

Since K_m/I_m is decreasing on $(0, +\infty)$, it suffices to show that for all $x > 0$,

$$\frac{K_m(x)}{I_m(x)} > \frac{K_m(x) + cK'_m(x)}{I_m(x) + cI'_m(x)},$$

and this follows immediately since $K'_m(x) < 0$ and $I'_m(x) > 0$. Similarly, the denominator of $a(m,k)$ is positive if and only if

$$\frac{-K'_m(x)}{I'_m(x)} > -\chi = \frac{-K_m(x+h) - cK'_m(x+h)}{I_m(x+h) + cI'_m(x+h)}.$$

Since

$$\frac{-K'_m(x)}{I'_m(x)} = \frac{K_{m-1}(x) + K_{m+1}(x)}{I_{m-1}(x) + I_{m+1}(x)}$$

is decreasing in $(0, +\infty)$, it suffices to show that for all $x > 0$,

$$\frac{-K'_m(x)}{I'_m(x)} > \frac{-K_m(x) - cK'_m(x)}{I_m(x) + cI'_m(x)},$$

and this follows immediately since $K_m(x) > 0$ and $I_m(x) > 0$. □

Thus, all hypotheses of Theorem 1 are satisfied by our application.

The idea here is again to use an optimized value p^* found in the range (11) for the explicit RN scheme (Algorithm 1 with $\alpha_s = 0$).

4 Numerical results

In this section we report numerical results aiming at showing the effectiveness of our proposal for the interface Robin parameters in the explicit RR and RN schemes. In particular, we want to understand if the values of the parameters derived by the simplified FSI problem (see Algorithm 2) work well for the complete three-dimensional FSI problem (1) solved by means of Algorithm 1. The use of simplified FSI models to perform analyses whose results are then used for more complex problems is a standard procedure due to the difficulty in analysing directly such problems. For example, simplified FSI problems have been used to study the convergence of strongly coupled partitioned procedures, then successfully tested over 3D general problems, in [2, 8, 9, 17, 20], and to derive the well-known result about the instability of the explicit Dirichlet-Neumann scheme for large added-mass effect in [8, 15].

All the simulations are run in the hemodynamic regime, characterized by a large added mass effect and where the stability of loosely-coupled methods is a challenging issue.

We consider problem (1) and for its time discretization we used the BDF schemes of order 1 for both fluid and structure, with a semi-implicit treatment of the fluid convective term. For the space discretization we used $P1bubble - P1$ Finite Elements for the fluid and $P1$ Finite Elements for the structure. The fluid domain at each time step is obtained by extrapolation of the previous time step (semi-implicit approach [3, 14, 26]). We also used the following data: fluid density $\rho_f = 1\, g/cm^3$, fluid viscosity $\mu = 0.035\, g/(cm\, s)$, structure density $\rho_s = 1.1\, g/cm^3$, Young modulus $E = 3 \cdot 10^5\, Pa$, Poisson ratio $\nu = 0.49$.

Notice that to compute $A(m, k)$ given by (6a) which is needed for the calibration of the interface parameters, we need the value of λ in the wave equation representing the structure problem in the simplified FSI problem. To do this, we assumed that the value of λ could be approximated by $G\lambda_1$, with $G = \pi^2/12$ the Timoshenko correction factor.

The fluid domain is a cylinder with length $L = 5\,cm$ and radius $R = 0.5\,cm$, whereas the structure domain is the external cylindrical crown with thickness $H_s = 0.1\,cm$. The meshes are composed by 4680 tetrahedra and 1050 vertices for the fluid and 1260 vertices for the structure.

At the inlet we prescribed a Neumann condition

$$\boldsymbol{T}_f(\boldsymbol{u}^{n+1}, p^{n+1})\boldsymbol{n} = -P_{in}\boldsymbol{n}, \tag{13}$$

with the following pressure function

$$P_{in} = \widehat{P}\left(1 - \cos\left(\frac{2\pi t}{0.01}\right)\right)\ dyne/cm^2, \quad t \leq T = 0.04\,s,$$

with absorbing resistance conditions at the outlets [25, 27].

If not otherwise specified, we used the following parameters (referred to as "basic"): $\widehat{P} = 500$, $\Delta t = 0.0005\,s$, $\gamma_{ST} = 1.5 \cdot 10^5\,Pa/cm$. All the numerical results have been obtained with the parallel Finite Element library `LIFEV` [1].

We will refer to RR-explicit simulation when using α_f and α_s selected in the range (8) described in Sect 3.2, whereas to RN-explicit simulation when using α_f in the range (11) as in Sect. 3.3 and $\alpha_s = 0$. We reported also the numerical solution obtained by using an implicit method, in particular the Robin-Neumann scheme, with an absolute tolerance of 10^{-7} on the convergence of the interface conditions.

In Table 1 we reported the values of the optimized Robin interface parameters a priori estimated via an empirical procedure. In particular, we take $K = [m_{min}, m_{max}] \times [k_{min}, k_{max}]$ with $m_{min} = 0$ and $m_{max} = 10$, $k_{min} = \pi/L = 0.6$ and $k_{max} = \pi/h = 13$ (remember that m and k are the angular and longitudinal frequencies) and we empirically look for p that minimizes $\max_{(m,k)\in K} \rho(m,k)$ when either $\alpha_f = p$, $\alpha_s = 2\overline{M} - p$ and p varies in the range (8) (RR-explicit), or $\alpha_f = p$, $\alpha_s = 0$ and p satisfies (11) (RN-Explicit). Notice from the analyses reported in Sections 3.2 and 3.3 that any change of Δt and γ_{ST} influences the estimates of the interface parameters, whereas the choice of $\widehat{P}$ does not.

	α_f - RR-expl	α_s - RR-expl	α_f - RN-expl
Basic	1045	-169	1084
$\Delta t = 10^{-3}$	1702	-115	1708
$\Delta t = 2.5 \cdot 10^{-4}$	866	-276	904
$\gamma_{ST} = 3 \cdot 10^5$	1526	-138	1590

Table 1: Values of the Robin interface parameters used in the loosely-coupled schemes.

In Figure 1 we report the time behaviour of the mean pressure at the section located at half of the pipe ($z = 2.5\,cm$) for different values of Δt.

In Figure 2 instead we show the same quantity in the case of an increased Reynolds number ($\widehat{P} = 5000$) for two values of the surrounding tissue parameter ($\gamma_{ST} = 3 \cdot 10^5\, Pa/cm$).

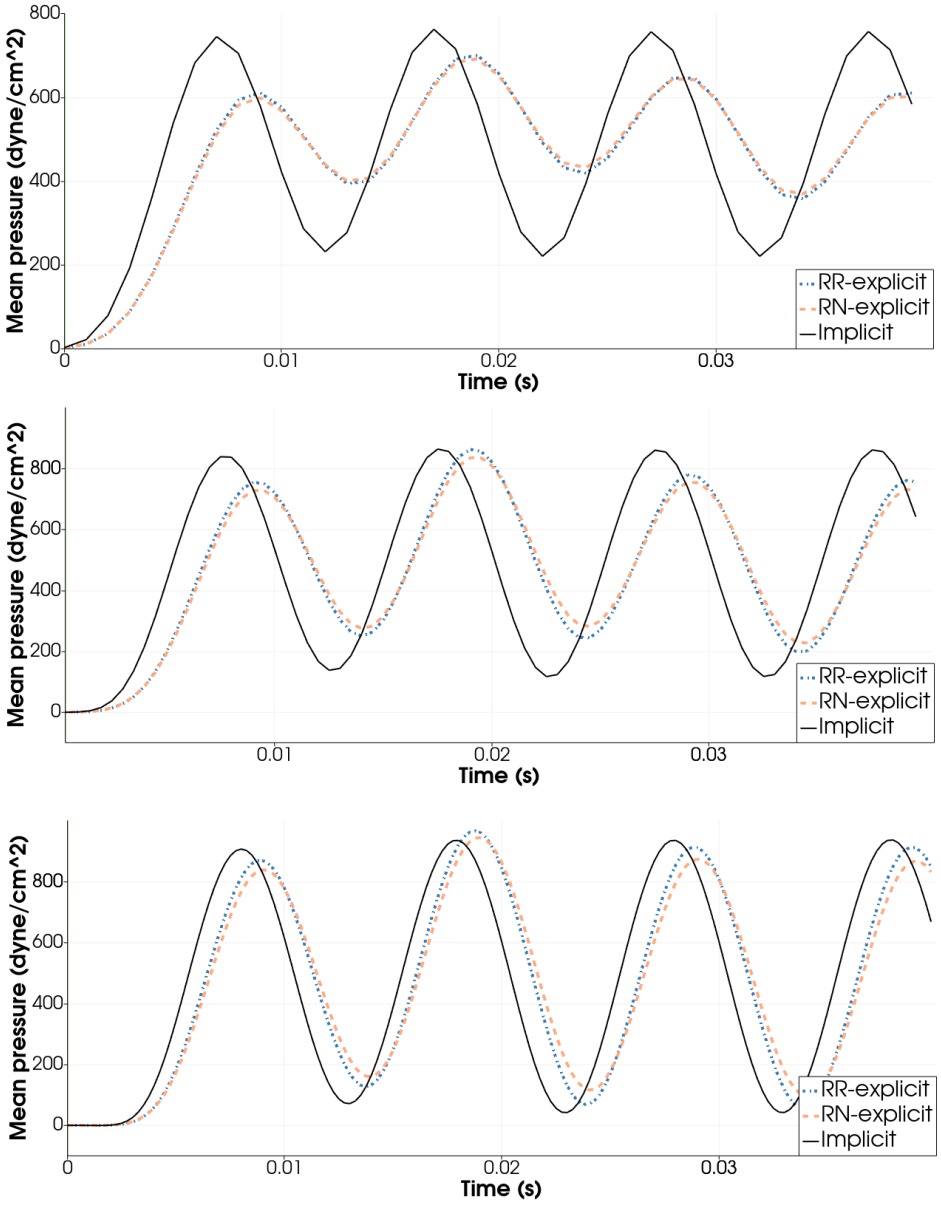

Figure 1: Mean pressure at section $z = 2.5\, cm$ for different values of Δt. Top: $\Delta t = 0.001\, s$; Middle: $\Delta t = 0.0005\, s$; Bottom: $\Delta t = 0.00025\, s$.

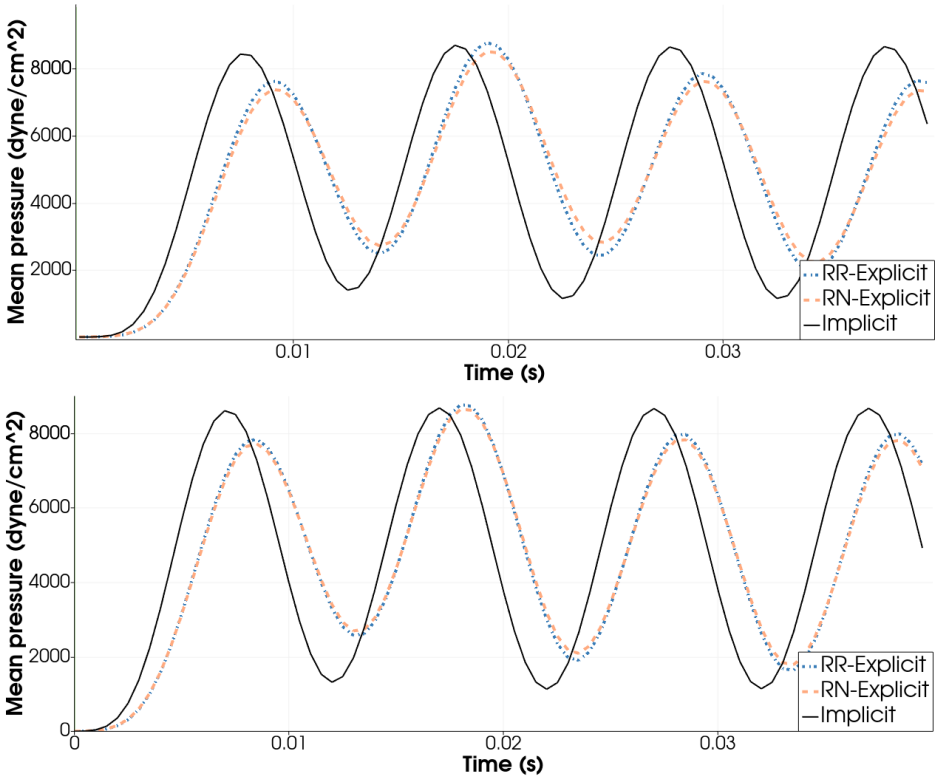

Figure 2: Mean pressure at section $z = 2.5\,cm$ for $\widehat{P} = 5000$ and $\Delta t = 0.0005\,s$, with $\gamma_{ST} = 1.5 \cdot 10^5$ (top) and $\gamma_{ST} = 3 \cdot 10^5$ (bottom).

From these results, we observe that the RR-Explicit and RN-Explicit solutions are in any case stable and feature a behaviour which is reasonable if compared with the implicit solution, also depicted in the figures. As expected, decreasing Δt the two solutions tend to coincide with the implicit one, see Figure 1. Also, from Figure 2 we notice that the performances of the proposed explicit schemes seem to be robust with respect to the Reynolds number and the value of the surrounding tissue. In any case, the two explicit solutions seem to be very similar, thus the new strategy proposed in Sect. 3.3 to estimate the fluid Robin parameter could be an effective way to build a loosely-coupled scheme characterized by only one parameter.

In the second test, we consider a human carotid reconstructed from MRI images. At the inlet we prescribed the Neumann condition (13) with

$$P_{in} = \begin{cases} 1000\ dyne/cm^2 & t \leq T = 0.005\,s, \\ 0\ dyne/cm^2 & 0.005\,s < t \leq 0.1, \end{cases}$$

with absorbing resistance conditions at the outlets. For the structure we imposed the Robin condition (1b) with $\gamma_{ST} = 3{\cdot}10^5\ Pa/cm$ at the external surface, homogeneous Neumann condition in the radial direction and homogeneous Dirichlet

condition in the tangential directions at the inlet, and fixed outlets. We set $\Delta t = 0.001\, s$. For the numerical solution, we considered the explicit RR scheme with parameters estimated as in Section 3.2. In particular, we used the values $\alpha_f = 4375$, $\alpha_s = -1287$ estimated by using the radius of the inlet in the analysis.

In Figure 3 we report the fluid and structure computational meshes, characterized by about 80k d.o.f for the fluid velocity, 10k d.o.f. for the fluid pressure, and 35k for the structure displacements. In Figure 4 we show the pressure filed in the deformed domain (amplified to be appreciated) at four representative time instants.

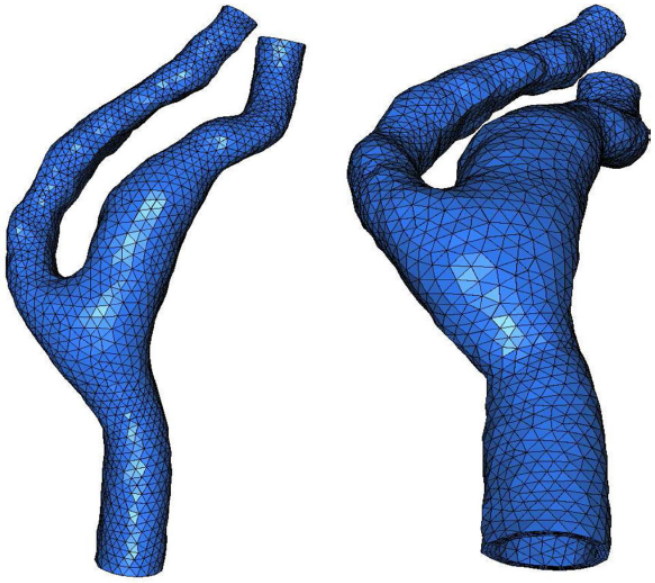

Figure 3: Fluid (left) and structure (right) computational meshes for the carotid simulation.

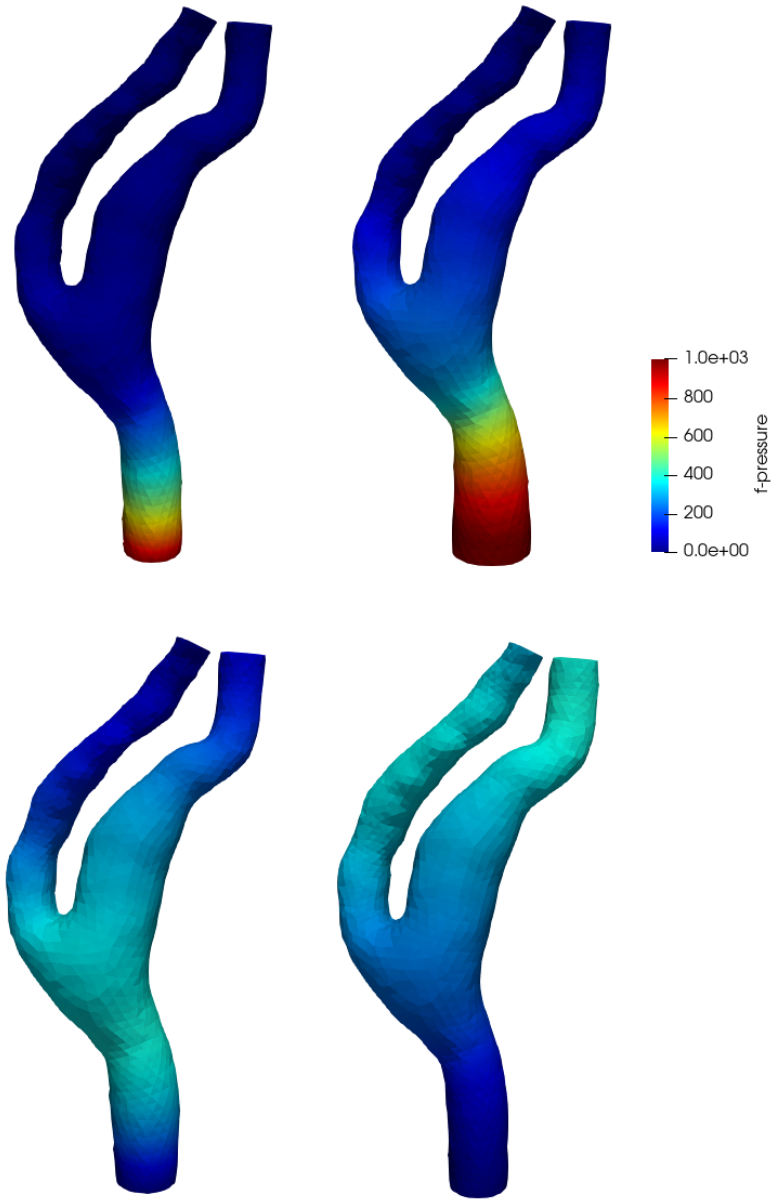

Figure 4: Pressure field in the deformed domain for the carotid simulation. Top, left: $t = 0.001$; Top, right: $t = 0.003$; Bottom, left: $t = 0.005$; Bottom, right: $t = 0.01$. Explicit RR simulation.

This is the first result obtained with the proposed explicit RR scheme in a real geometry in the context of hemodynamics. The results are stable and highlight the ability of the method of representing the wave propagation and the deformation of the domains. Although the prescribed data at the inlet is not physiological, this test gives an important preliminary answer toward the use

of explicit Robin-Robin and Robin-Neumann methods for clinical applications, with a dramatic save in computational times with respect to strongly-coupled (implicit) schemes.

Acknoowledgments

C. Vergara has been partially supported by the H2020-MSCA-ITN-2017, EU project 765374 "ROMSOC - Reduced Order Modelling, Simulation and Optimization of Coupled systems" and by the Italian research project MIUR PRIN17 2017AXL54F. "Modeling the heart across the scales: from cardiac cells to the whole organ".

References

[1] Lifev user manual, `http://lifev.org`, 2010.

[2] S. Badia, F. Nobile, and C. Vergara. Fluid-structure partitioned procedures based on Robin transmission conditions. *J. Comput. Physics*, 227:7027–7051, 2008.

[3] S. Badia, A. Quaini, and A. Quarteroni. Splitting methods based on algebraic factorization for fluid-structure interaction. *SIAM J Sc Comp*, 30(4):1778–1805, 2008.

[4] J.W. Banks, W.D. Henshaw, and D.W. Schwendeman. An analysis of a new stable partitioned algorithm for fsi problems. part i: Incompressible flow and elastic solids. *J. Comput. Physics*, 269:108–137, 2014.

[5] M. Bukac, S. Canic, R. Glowinski, B. Muha, and A. Quaini. A modular, operator-splitting scheme for fluid–structure interaction problems with thick structures. *Int. J. Num. Meth. Fluids*, 74(8):577–604, 2014.

[6] M. Bukac, S. Canic, R. Glowinski, J. Tambaca, and A. Quaini. Fluid–structure interaction in blood flow capturing non-zero longitudinal structure displacement. *J. Comput. Physics*, 235:515–541, 2013.

[7] E. Burman and M.A. Fernández. Explicit strategies for incompressible fluid-structure interaction problems: Nitsche type mortaring versus robin–robin coupling. *Int. J. Num. Methods Engrg.*, 97:739–758, 2014.

[8] P. Causin, J.F. Gerbeau, and F. Nobile. Added-mass effect in the design of partitioned algorithms for fluid-structure problems. *Comput. Methods Appl. Mech. Engrg.*, 194(42-44):4506–4527, 2005.

[9] W.G. Dettmer, A. Lovric, C. Kadapa, and D. Peric. New iterative and staggered solution schemes for incompressible fluid-structure interaction based on dirichlet-neumann coupling. *Int. J. Num. Methods Engrg.*, pages 1 – 32, 2020.

[10] J. Donea. An arbitrary Lagrangian-Eulerian finite element method for transient dynamic fluid-structure interaction. *Comput. Methods Appl. Mech. Engrg.*, 33:689–723, 1982.

[11] C. Farhat, K.G. van der Zee, and P. Geuzaine. Provably second-order time-accurate loosely-coupled solution algorithms for transient nonlinear computational aeroelasticity. *Comput. Methods Appl. Mech. Engrg.*, 195:1973–2001, 2006.

[12] M. Fernandez, J. Mullaert, and M. Vidrascu. Explicit robin–neumann schemes for the coupling of incompressible fluids with thin-walled structures. *Comput. Methods Appl. Mech. Engrg.*, 267:566–593, 2013.

[13] M.A. Fernández. Incremental displacement-correction schemes for incompressible fluid-structure interaction - stability and convergence analysis. *Numerische Mathematik*, 123(1):21–65, 2013.

[14] M.A. Fernández, J.F. Gerbeau, and C. Grandmont. A projection semi-implicit scheme for the coupling of an elastic structure with an incompressible fluid. *Int. J. Num. Methods Engrg.*, 69(4):794–821, 2007.

[15] C. Forster, W. Wall, and E. Ramm. Artificial added mass instabilities in sequential staggered coupling of nonlinear structures and incompressible viscous flow. *Comput. Methods Appl. Mech. Engrg.*, 196(7):1278–1293, 2007.

[16] M.J. Gander. Optimized Schwarz methods. *SIAM J. Numer. Anal.*, 44(2):699–731, 2006.

[17] L. Gerardo Giorda, F. Nobile, and C. Vergara. Analysis and optimization of robin-robin partitioned procedures in fluid-structure interaction problems. *SIAM J. Numer. Anal.*, 48(6):2091–2116, 2010.

[18] G. Gigante, G. Sambataro, and C. Vergara. Optimized schwarz methods for spherical interfaces with application to fluid-structure interaction. *SIAM J. Sci. Comp.*, 42(2):A751–A770, 2020.

[19] G. Gigante and C. Vergara. Analysis and optimization of the generalized schwarz method for elliptic problems with application to fluid-structure interaction. *Numer. Math.*, 131(2):369–404, 2015.

[20] G. Gigante and C. Vergara. On the stability of a loosely-coupled scheme based on a robin interface condition for fluid-structure interaction. *ArXiv*, page 1905.06593, 2019.

[21] G. Guidoboni, R. Glowinski, N. Cavallini, and S. Canic. Stable loosely-coupled-type algorithm for fluid–structure interaction in blood flow. *J. Comput. Physics*, 228:6916–6937, 2009.

[22] N. Lebedev. *Special Functions and Their Applications*. Courier Dover Publications, 1972.

[23] M. Lukacova-Medvid'ova, G.Rusnakova, and A.Hundertmark-Zauskova. Kinematic splitting algorithm for fluid–structure interaction in hemodynamics. *Comput. Methods Appl. Mech. Engrg.*, 265:83–106, 2013.

[24] P. Moireau, N. Xiao, M. Astorino, C. A. Figueroa, D. Chapelle, C. A. Taylor, and J.F. Gerbeau. External tissue support and fluid–structure simulation in blood flows. *Biomechanics and Modeling in Mechanobiology*, 11(1–2):1–18, 2012.

[25] F. Nobile, M. Pozzoli, and C. Vergara. Time accurate partitioned algorithms for the solution of fluid-structure interaction problems in haemodynamics. *Computer & Fluids*, 86:470–482, 2013.

[26] F. Nobile, M. Pozzoli, and C. Vergara. Inexact accurate partitioned algorithms for fluid-structure interaction problems with finite elasticity in haemodynamics. *Journal of Computational Physics*, 273:598–617, 2014.

[27] F. Nobile and C. Vergara. An effective fluid-structure interaction formulation for vascular dynamics by generalized Robin conditions. *SIAM J Sc Comp*, 30(2):731–763, 2008.

[28] F. Nobile and C. Vergara. Partitioned algorithms for fluid-structure interaction problems in haemodynamics. *Milan Journal of Mathematics*, 80(2):443–467, 2012.

[29] K.C. Park, C.A. Felippa, and J.A. De Runtz. Stabilisation of staggered solution procedures for fluid-structure interaction analysis. *Comput. Methods Appl. Mech. Engrg.*, 26, 1977.

[30] S. Piperno and C. Farhat. Partitioned prodecures for the transient solution of coupled aeroelastic problems-Part II: energy transfer analysis and three-dimensional applications. *Comput. Methods Appl. Mech. Engrg.*, 190:3147–3170, 2001.

[31] A. Quarteroni, A. Manzoni, and C. Vergara. The cardiovascular system: Mathematical modelling, numerical algorithms and clinical applications. *Acta Numerica*, 26:365–590, 2017.

[32] E.W. Swim and P. Seshaiyer. A nonconforming finite element method for fluid-structure interaction problems. *Comput. Methods Appl. Mech. Engrg.*, 195(17–18):2088–2099, 2006.

MOX Technical Reports, last issues

Dipartimento di Matematica
Politecnico di Milano, Via Bonardi 9 - 20133 Milano (Italy)

16/2021 Salvador, M.; Dede', L.; Manzoni, A.
Non intrusive reduced order modeling of parametrized PDEs by kernel POD and neural networks

17/2021 Chew, R.; Benacchio, T.; Hastermann, G.; Klein, R.
Balanced data assimilation with a blended numerical model

13/2021 Ferro, N.; Perotto, S.; Cangiani, A.
An anisotropic recovery-based error estimator for adaptive discontinuous Galerkin methods

14/2021 Peli, R.; Menafoglio, A.; Cervino, M.; Dovera, L.; Secchi, P;
Physics-based Residual Kriging for dynamically evolving functional random fields

15/2021 Fumagalli, A.; Patacchini, F.S.
Model adaptation in a discrete fracture network: existence of solutions and numerical strategies

10/2021 Di Michele, F.; May, J.; Pera, D.; Kastelic, V.; Carafa, M.; Smerzini, C.; Mazzieri, I.; Rubino,
Spectral elements numerical simulation of the 2009 L'Aquila earthquake on a detailed reconstructed domain

11/2021 Antonietti,P.F.; Manzini, G.; Mazzieri, I.; Scacchi, S.; Verani, M.
The conforming virtual element method for polyharmonic and elastodynamics problems: a review

12/2021 di Cristofaro, D.; Galimberti, C.; Bianchi, D.; Ferrante, R.; Ferro, N.; Mannisi, M.; Perotto, S
Adaptive topology optimization for innovative 3D printed metamaterials

09/2021 Riccobelli, D.; Noselli, G.; DeSimone, A.
Rods coiling about a rigid constraint: Helices and perversions

08/2021 Antonietti, P. F.; Manuzzi, E.
Refinement of polygonal grids using Convolutional Neural Networks with applications to polygonal Discontinous Galerkin and Virtual Element methods